PROTEINS: Structure, Function, and Bioinformatics 66:229–238 (2007)

High Resolution Crystal Structures of Unliganded and Liganded Human Liver ACBP Reveal a New Mode of Binding for the Acyl-CoA Ligand

Jukka P. Taskinen,[1] Daan M. van Aalten,[2] Jens Knudsen,[3] and Rik K. Wierenga[1]*
[1]*Biocenter Oulu and Department of Biochemistry, University of Oulu, FIN-90014, Finland*
[2]*School of Life Sciences, University of Dundee, Dundee DD1 5EH, United Kingdom*
[3]*Department of Biochemistry and Molecular Biology, University of Southern Denmark, Campusvej 55, DK-5230 Odense M, Denmark*

ABSTRACT **The acyl-CoA binding protein (ACBP) is essential for the fatty acid metabolism, membrane structure, membrane fusion, and ceramide synthesis. Here high resolution crystal structures of human cytosolic liver ACBP, unliganded and liganded with a physiological ligand, myristoyl-CoA are described. The binding of the acyl-CoA molecule induces only few structural differences near the binding pocket. The crystal form of the liganded ACBP, which has two ACBP molecules in the asymmetric unit, shows that in human ACBP the same acyl-CoA binding pocket is present as previously described for the bovine and *Plasmodium falciparum* ACBP and the mode of binding of the 3′-phosphate-AMP moiety is conserved. Unexpectedly, in one of the acyl-CoA binding pockets the acyl moiety is bound in a reversed mode as compared with the bovine and *P. falciparum* structures. In this binding mode, the myristoyl-CoA molecule is fully ordered and bound across the two ACBP molecules of the crystallographic asymmetric unit: the 3′-phosphate-AMP moiety is bound in the binding pocket of one ACBP molecule and the acyl chain is bound in the pocket of the other ACBP molecule. The remaining binding pocket cavities of these two ACBP molecules are filled by other ligand fragments. This novel binding mode shows that the acyl moiety can flip out of its classical binding pocket and bind elsewhere, suggesting a mechanism for the acyl-CoA transfer between ACBP and the active site of a target enzyme. This mechanism is of possible relevance for the in vivo function of ACBP. Proteins 2007;66:229–238.** © 2006 Wiley-Liss, Inc.

Key words: ACBP; CoA; myristoyl-CoA; SCP2; FABP

INTRODUCTION

Acyl-CoA thioesters are molecules with many fundamental roles in cellular processes. The intracellular concentration of free fatty acyl-CoA molecules is tightly controlled in the range of about 0.1–200 n*M* under normal physiological conditions.[1] The balance between free fatty acids and their CoA-derivatized counterparts in soluble and protein bound pools is regulated by a number of proteins, like sterol carrier protein 2 (SCP-2), fatty acid binding protein (FABP), and acyl-CoA binding protein (ACBP). The majority of the cellular acyl-CoA is bound by ACBP.[2]

ACBP is known as a cytosolic, monomeric 10 kDa protein, and homologues have been found in all eukaryotic kingdoms and in some eubacterial species.[2] In eukaryotes, ACBP is a cytosolic protein with access to the nuclear compartment. In mammals, three isoforms have been identified: L-ACBP, T-ACBP, and B-ACBP from liver, testes, and brain, respectively, and six isoforms have been found in *Drosophila melanogaster*.[3,4] ACBP has a well-conserved amino acid sequence of 86–103 amino acids, and the high sequence conservation of the ACBP[4] as well as its ubiquitous expression suggest that ACBP has essential physiological functions. In addition to independent protein entities, database searches using the ACBP amino acid sequence as a probe have suggested that ACBP-like domains may also occur as a part of larger proteins, for example, in membrane associated proteins,[5] β-oxidation enzymes having both ACBP and enoyl-Δ^3,Δ^2-CoA isomerase domains,[6] and proteins with an ACBP domain and an ankyrin repeat.[7] In the structure of FERM (band four-point-one ezrin–radixin–moesin homology domains), a family of proteins that localize proteins into plasma membrane, the ACBP-like domain is present in an inactive form as the F2 domain.[8]

ACBP has been discovered recently[9] and only limited structural information is available. Its four helical bundle structure was first observed in the NMR structure of the unliganded bovine ACBP (bL-ACBP) in 1991.[10] The topology of this up–down–down–up bundle is unique for the four helical bundle domains. The three-dimensional NMR structure of the liganded bovine ACBP with palmitoyl-

Grant sponsors: Wellcome Trust Senior Research Fellowship, EMBO YIP, Sigrid Jusélius Foundation.

*Correspondence to: Rik Wierenga, Department of Biochemistry, P.O. Box 3000, University of Oulu, FIN-90014, Finland.
E-mail: rik.wierenga@oulu.fi

Received 23 February 2006; Revised 16 May 2006; Accepted 15 June 2006

Published online 16 October 2006 in Wiley InterScience (www.interscience.wiley.com). DOI: 10.1002/prot.21124

Fig. 1. Structural sequence alignment of human, bovine, and *P. falciparum* ACBP. Helices A1, A2, A3, and A4 are illustrated as labeled cylinders above the sequences. In the monomeric binding mode, the residues of chain B interacting with the adenine ring are labeled with a vertical bar, residues interacting with the 3′-phosphate moiety are labeled with a triangle, residues interacting with the acyl moiety are marked with a curly line, and hydrophobic residues close to the ω-end of the acyl chain (shaping the tunnel near the N-termini of helices A2 and A3) are marked with a black circle. The black squares mark the three residues of chain A which interact with the 3′-phosphate-ribose moiety in the dimeric mode of binding.

CoA has also been described in detail.[11] Crystal structures have been published for bovine apo ACBP[12] and for myristoyl-CoA complexed *Plasmodium falciparum* ACBP (Pf-ACBP).[12] The very simple structure of ACBP has also made possible NMR studies on its folding and unfolding properties.[13]

The amino acid sequences of the ACBPs of known structure, including the sequence of the human ACBP (hL-ACBP), are listed in Figure 1. All known structures have the same four-helix bundle fold (helices A1, A2, A3, and A4), with a 13-residue loop insertion between the parallel helix-pair of A2 and A3. Helices A1 and A4 are also assembled as two parallel helices (Fig. 2).

Binding of fatty acyl-CoAs to the ACBP occurs with a very high affinity (K_D = 1–5 n*M*). The 3′-phosphate interactions in the CoA end of the ligand account for 40% of the total binding energy,[14,15] and only CoA-derivatized fatty acids are bound to ACBP. In the NMR structure of liganded bovine L-ACBP, the acyl-CoA molecule is bound to the protein in a spiral-like conformation. Conceptually, the acyl-CoA binding pocket can be divided into three parts as shown in Figure 2: (i) the adenine ring binding pocket created by a tyrosine residue (Tyr32 in hL-ACBP) and the acyl moiety of the acyl-CoA molecule; (ii) the 3′-phosphate binding site composed of a set of hydrogen bonding and positively charged residues (Tyr29, Lys33, and Lys55 in hL-ACBP) providing hydrogen bonds with phosphate oxygen atoms; and (iii) a hydrophobic groove for binding the acyl moiety extending from the C-terminus of helix A1 (near hL-ACBP Arg14) to the N-termini of helices A2 (near hL-ACBP Met25 and Leu26) and A3 (near hL-ACBP Ala54 and Lys55) near the ω-end of the acyl moiety. The pantetheine moiety of the acyl-CoA is exposed to the solvent and disordered in the crystal structure of Pf-ACBP complex.

Here we describe the high resolution structures of the unliganded and liganded liver isoform of human L-ACBP. The ligand used in these studies is myristoyl-CoA, in which the acyl chain moiety is a saturated C_{14} carboxylic acid. This is the third structural report on the binding properties of ACBP and the first report on the structure of a human ACBP. The liganded structure has been crystallized as a dimer in the asymmetric unit, referred to as molecules A and B, and one of the myristoyl-CoA ligands binds with its adenine part to molecule B, whereas the ω-end of its acyl chain is bound to molecule A of this dimer. The possible relevance for the in vivo functionality of this mode of binding is discussed.

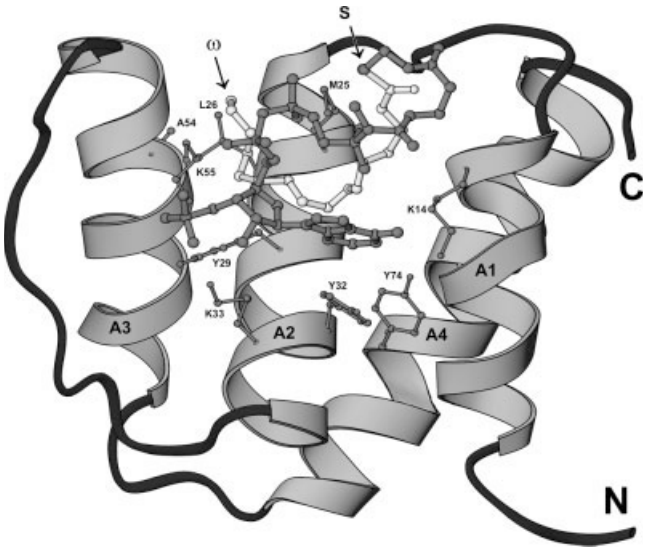

Fig. 2. Schematic drawing of the structure of bovine ACBP complexed with palmitoyl-CoA. The palmitoyl-CoA is drawn as a grey ball-and-stick model, except the fatty acyl moiety, which is shown in white. S labels the sulfur of the CoA moiety and ω shows the ω-end of the acyl moiety. The adenine ring is stacked between the acyl moiety and Tyr32. The other side chains also interact with the ligand in the monomeric binding mode, as identified in Figure 1 (numbering follows the hL-ACBP sequence, K14 corresponds to Arg14 of the hL-ACBP). N and C label the N-terminus and C-terminus of the polypeptide chain. The helices are labeled as A1, A2, A3, and A4.

MATERIALS AND METHODS

Crystallization and Data Collection of the Apo Protein

The protein was purified similarly as described previously for bovine ACBP.[16] Lyophilized protein was dissolved to a final concentration of 20 mg/mL in 50 m*M* MES, pH 7.0, 50 m*M* NaCl. Prior to crystallization experiments, $Pb(NO_3)_2$ was added to a final concentration of 5 m*M*, as it has been established by in vivo studies that human ACBP is one of the proteins that binds lead ions with high affinity.[17] The screening for crystallization conditions was initiated using Hampton Research Crystal Screens I and II and the hanging drop method.[18] In screening, 1 μL of protein solution was mixed with 1 μL of the well solution and suspended over 500 μL of the well solution. After 3 h at +4°C, microcrystals were observed in conditions consisting of 25% PEG-MME 550, 100 m*M* MES, pH 6.5, 10 m*M* $ZnSO_4$, and 3% 1-propanol. Larger crystals were obtained using the following seeding protocol. Single microrystals

TABLE I. Data Collection Statistics

	Apo	Myr-CoA	Myr-CoA	Myr-CoA
Wavelength (Å)	0.91	0.93	1.2818	1.7453
Temperature (K)	100	100	100	100
Space group	$P6_522$	$I23$	$I23$	$I23$
Unit cell (Å)				
a	43.89	118.49	118.31	119.83
b	43.89	118.49	118.31	119.83
c	177.57	118.49	118.31	119.83
Resolution (Å)	30–1.56	19–1.35	25–2.26	25–2.35
Highest bin (Å)	1.62–1.56	—	2.36–2.26	2.43–2.35
Redundancy	4.6	5.4	4.3	3.6
Completeness (%)	96.1 (98.5)	99.8	98.4 (99.3)	92.9 (84.4)
R_{merge} (%)	5.2 (21.1)	6.5	8.9 (35.5)	4.1 (15.9)
I/σ	31.9 (6.1)	13.9	13.3 (9.6)	23.8 (5.5)

were transferred to similar drops as above, but not containing any 1-propanol. Before receiving the seeds, these drops were pre-equilibrated against the well solution for 10 h at +4°C; during this pre-equilibration, a heavy precipitate was observed. After transfer into the pre-equilibrated drops, the microcrystals increased in size and single crystals with dimension of approximately $0.1 \times 0.1 \times 0.1$ mm^3 were harvested with a nylon CryoLoop (Hampton Research, CA) after 10 h and flash frozen in a 100 K nitrogen stream (Oxford Cryostream Cooler). No additional cryoprotectant was required.

The data collection was carried out from a single crystal to 1.6 Å resolution at beam line X11 at the EMBL outstation at the DESY synchrotron, Hamburg, Germany. 0.5° oscillations were exposed on MAR CCD detector using a wavelength of 0.91 Å. Indexing and scaling of the images with the HKL suite[19] suggested the space group to be $P6_522$ or $P6_122$, with the unit cell parameters $a = b = 43.89$ Å, $c = 177.57$ Å. The Matthews coefficient V_m is 2.6 Å^3/Da for one monomer per asymmetric unit. 3.5% of the reflections were flagged for the R_{free} set.[20] Data collection statistics are shown in Table I.

Crystallization and Data Collection of the Myristoyl-CoA Complex

The lyophilized protein was dissolved to a 15 mg/mL solution in 50 m*M* MES, pH 7.0, 50 m*M* NaCl. Myristoyl-CoA (Sigma), suspended into water, was added to a concentration of approximately 1.8 m*M*. The crystallization screening was performed as above. Single crystals were grown from conditions consisting of 24% PEG-MME 550, 100 m*M* MES, pH 6.5, 10 m*M* $ZnSO_4$. The native 1.4 Å dataset was collected from one crystal, which was cryoprotected by soaking for approximately 30 sec in mother liquor with increased (35%) PEG-MME 550 concentration before flash freezing. Data collection was carried out at the beam line ID14-4 at the European Synchrotron Radiation Facility, Grenoble. Oscillations of 0.5° were exposed on the ADSC Q4 CCD detector. Data processing was performed with the program XDS,[21] and it suggested the space group to be $I23$ or $I2_13$, with the unit cell parameters $a = b = c =$ 118.5 Å. V_m is 3.6 Å^3/Da for two monomers per asymmetric unit. Data collection statistics are presented in Table I.

Structure Determination and Refinement of the Apo Structure

The heavy metal atoms were located using the CNS package[22] resulting in one Pb^{2+} site and one Zn^{2+} site. To improve the phases, density modification was performed using the "solvent flipping" method as implemented in CNS. The phases were combined with the initial amplitudes of the structure factors and together with the heavy atom positions they were used as an initial model in the ARP/WARP[23] program for automated model building. The correct space group was found to be $P6_522$.

Refinement was further continued using the CNS package. Manual model building was done with the program O[24]; alternate side chain conformations and ordered water molecules were added where appropriate. The structure was validated with PROCHECK[25] and WHATIF[26] during the refinement. Individual B-factors were refined for every atom. The final R/R_{free} are 19.3%/23.0% (Table II).

Structure Determination and Refinement of the Myristoyl-CoA Structure

Eight Zn^{2+} ions were located by the SAD method using CNS. After density modification with CNS, the initial electron density map was used in ARP/wARP[23] for automatic model building. The asymmetric unit contains two monomers: monomer A (near the crystallographic threefold axis) and monomer B. Using this approach the correct space group was found to be $I23$.

The initial model was refined using CNS. O was used to manually adjust the side chain conformations and to add residues missing from the model. Further refinement was done with Refmac5.[27] After including all side chains, TLS refinement[28] was carried out using each monomer as an individual TLS group. Peaks with positive electron density and a favorable hydrogen bonding network were identified as ordered water molecules and they were added in subsequent model building and refinement cycles to the

TABLE II. Refinement Statistic

	Apo	Myr-CoA
Resolution range (Å)	15–1.6	19–1.40
No. of reflections	14,765	54,202
No. of working set reflections	14,256	53,111
R factor (%)	19.3	17.0
R_{free} (%)	23.0	19.3
No. of protein atoms	698	1478
No. of water molecules	228	290
No. of sulfate molecules	0	1
No. of heavy metal ions	2	8
Geometry statistics		
Rmsd for bond distances (Å)	0.015	0.011
Rmsd for bond angles (deg)	1.50	1.85
Rmsd for B factors (Å^2)		
Main chain (A, B)	0.8	0.7, 0.8
Side chain (A, B)	2.1	2.3, 2.7
Average B factors (Å^2)[a]		
Protein atoms (A, B)	16.4	15.5, 15.7
Ligand atoms	—	31.1
Solvent atoms	33.8	41.2
Ramachandran plot		
Most favored (%)	94.5	95.4
Additionally allowed (%)	4.1	4.6
Generously allowed (%)	1.4	0.0
Disallowed (%)	0.0	0.0

[a]The contribution of the TLS parameters is not included in the *B* factors.

model, provided that they were not close to the putative ligand molecules or Zn^{2+} ions.

Three 3′-phosphate-AMP moieties of the ligand molecules had clear continuous density in the initial ($F_o - F_c$) α_c maps and these fragments were added in the model (molecules C1, D1, and P1; C1 is bound to monomer B, molecules D1 and P1 are complexed to monomer A). After adding these 3′-phosphate-AMP fragments, the R-factor was 17.3% ($R_{free} = 20.4\%$) at 1.8 Å resolution.

At this stage the ($F_o - F_c$) α_c difference maps clearly indicated the presence of additional ligand fragments as visualized in Figure 3(A). Continuous density was observed starting from the 5′-phosphate group of the C1 molecule and extending from molecule B toward molecule A. Also, a stretch of positive density corresponding to the carbon atoms of an acyl chain was observed in the acyl chain binding groove of monomer B, as is seen in Figure 3(A). Additional electron density was observed corresponding to a sulfate ion in the centre of the Zn^{2+} cluster. First, the residual density features corresponding to a full length myristoyl-CoA molecule (C1) were modeled. The data range was extended to 1.4 Å and anisotropic B-factors were refined for the protein atoms. Switching to anisotropic B-factor refinement resulted in a drop in R/R_{free} from 18.7%/21.0% to 16.8%/18.7% at 1.4 Å resolution. Subsequently, a sulfate was added inside the Zn^{2+} cluster and in the acyl chain binding groove of monomer B was modeled an acyl chain extended by the β-mercaptoethylamine fragment of the panthetheine moiety (molecule C2). This electron density for acyl chain did not connect to either of the two remaining 3′-phosphate-AMP fragments, indicating the presence of four myristoyl-CoA molecules per asymmetric unit (molecules C1, C2, D1, and P1) of which only molecule C1 corresponds to a complete myristoyl-CoA molecule, whereas C2 is only an acyl chain extended by a β-mercaptoethylamine fragment, and D1 and P1 are 3′-phosphate-AMP moieties. Finally, alternative conformations for some side chains were added when appropriate and more ordered water molecules with satisfactory hydrogen bonding network were added. At the end of the refinement the R-factor was 17.0% ($R_{free} = 19.3\%$) at 1.4 Å resolution. The refinement statistics are described in more detail in Table II.

Anomalous Difference Maps of the Myristoyl-CoA-hL-ACBP Crystal

To confirm the location of the heavy atoms in the myristoyl-CoA-hL-ACBP complex, two additional datasets were collected (Table I) from a single crystal at wavelengths appropriate for measuring the anomalous signal of Zn atoms ($\lambda = 1.2818$ Å) and of S and P atoms ($\lambda = 1.7453$ Å). The 1.4 Å structure of the myristoyl-CoA complex (using protein atoms only) was refined against these two datasets. When combined with calculated phases derived from the refined model, the eight highest anomalous difference peaks (28.7 σ – 9.7 σ; the next highest peak is 5.4 σ) from the 1.2818 Å dataset correspond to the positions of the eight Zn^{2+} ions used for the initial SAD-phasing. Similarly for the $\lambda = 1.7453$ Å data, the anomalous difference maps showed positive peaks at positions corresponding to Zn, S, and P atoms. One of the highest anomalous peaks (8.0 σ) in this anomalous difference map is in the centre of the Zn^{2+} cluster in good agreement with the presence of a sulfate ion. A high (4.0 σ) peak in this map corresponds to the position of the thioester sulfur of the full length myristoyl-CoA molecule (C1), thus confirming the extended mode of binding of this myristoyl-CoA, between the monomers A and B.

Mass Spectroscopy Analysis

The analysis of the electron density maps showed the presence of fragments of myristoyl-CoA arising either from a partly disordered mode of binding or because of the presence of these fragments in the crystallization solution. Consequently, myristoyl-CoA solutions similar as used in the crystallization setup were analyzed by mass spectroscopy. Using the electrospray ionization method in negative mode on a Q-TOFI (MicroMass) instrument, fragments corresponding to phosphopantetheine-myristoyl and 3′-phosphate-AMP were identified.

RESULTS

The Comparison of the Structures of Apo and Liganded Human L-ACBP

Crystal structures were determined of apo hL-ACBP (at 1.6 Å resolution) and liganded hL-ACBP (at 1.4 Å resolution). Both crystal forms were obtained by cocrystallization in the presence of metal ions; Zn^{2+} and Pb^{2+} for the apo structure and Zn^{2+} for the complex structure, respectively.

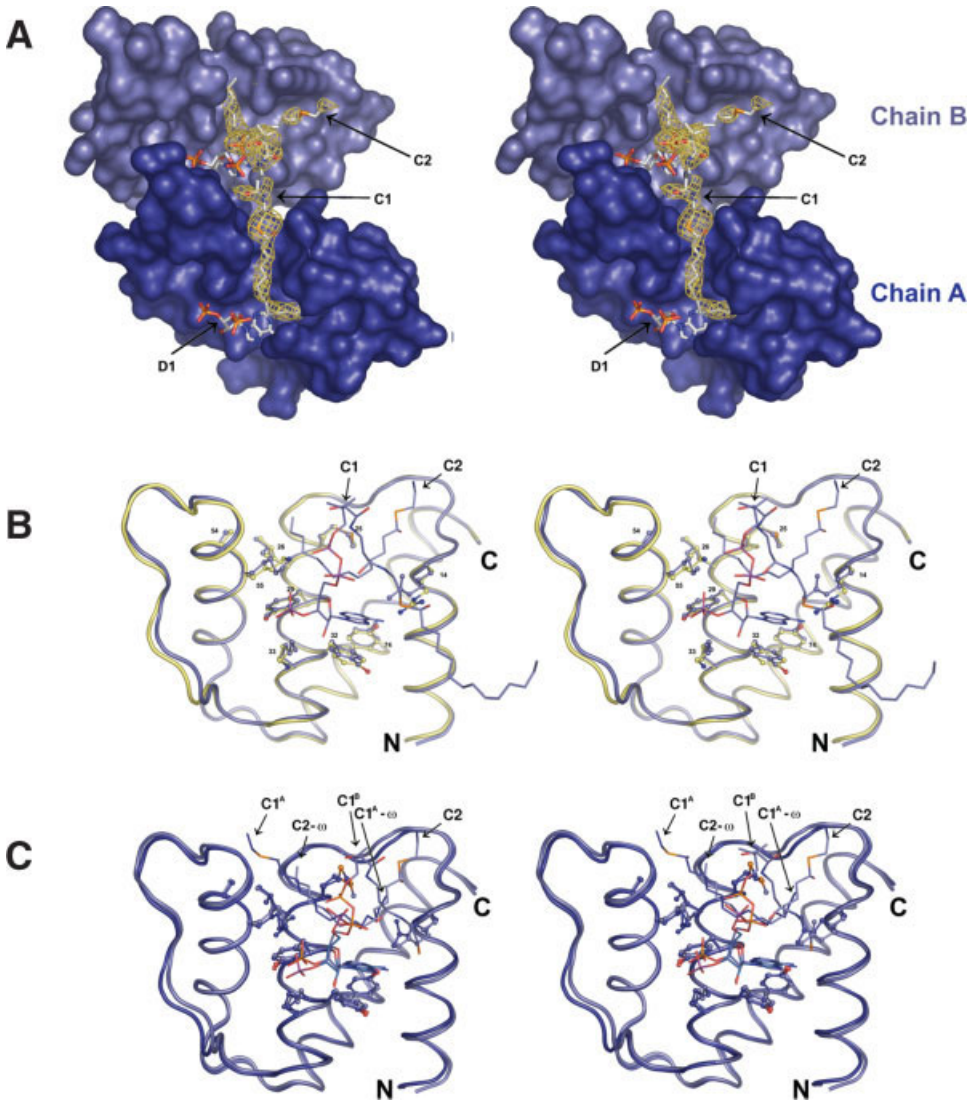

Fig. 3. The crystal structure of human ACBP. (**A**) Dimeric binding mode of the hL-ACBP-myristoyl-CoA complex. The molecular surfaces of chain A and B are shown as dark blue and light blue, respectively. The omit electron density represents the 2.5 σ ($F_o - F_c$) α_c density of the pantetheine-acyl moiety at a refinement step in which only 3′-phosphate AMP moieties of the ligands were included in the model. The omit density shows the ligand molecule C1 bound between the two monomers. The acyl binding groove shaped by residues of the loop between A1 and A2 is narrower in monomer A (binding the ω-end of the acyl moiety of molecule C1 in the dimeric mode of binding) than in monomer B (binding the β-mercaptoethylamine-acyl moiety of molecule C2 as in the classical monomeric mode of binding). (**B**) Comparison of chain B of the myristoyl-CoA-hL-ACBP complex (light blue) and the hL-ACBP apo structure (yellow). The adenine ring stacks on Tyr32 and hydrogen bonds to Arg14 and Tyr74. The 3′-phosphate hydrogen bonds to Tyr29, Lys33, and Lys55. The side chains of the "tunnel" residues Ala54, Lys55, Met25, and Leu26 are also shown and labeled with residue numbers. (**C**) Comparison of chain B (light blue) and chain A (dark blue) of the hL-ACBP-myristoyl-CoA complex. The orientation of the acyl moieties of C1 and C2 in the respective binding grooves of chain A and chain B are opposite but the same residues interact with the ligand. In the dimeric binding mode, the side chain of Arg14 of helix A1 (chain A) moves closer to Met25 (on the other side of the binding groove). Labels C1A and C1B show the binding of the ligand to chain A and chain B, respectively.

The apo crystals were obtained through a seeding protocol from transferred microcrystals. The apo structure contains one ACBP polypeptide chain (from residues Ser2 to Ile87) in the asymmetric unit. The apo structure was refined to the final $R = 19.3\%$ and $R_{free} = 23.0\%$. In the liganded form, two ACBP polypeptide chains are found per asymmetric unit complexed to four ligand molecules. Molecule A comprises residues Ser2 to Ile87 whereas molecule B comprises residues Gln3 to Ile87. Neither the apo nor the liganded structures have high B-factor loops. In both structures there are no residues in the disallowed regions of the Ramachandran plot. However, in the apo structure Met47 is in the generously allowed region ($\phi = 51^\circ$, $\psi = -134^\circ$). This residue, which is in the long loop just before helix A3,

has a relatively high B-factor but the electron density map agrees with this somewhat strained conformation. The methionine side chain points into the acyl binding pocket of a crystallographically related molecule. In the liganded molecules this loop adopts a slightly different conformation.

The structures of unliganded and liganded hL-ACBP after superposing are compared in Figure 3(B) using the C^{α}-atoms of the four helices for the superpositioning (the rmsd value for 51 corresponding C^{α} atoms is 0.3 Å). The side chains of the residues Arg14 and Tyr32 have adopted slightly different conformations when comparing the apo and liganded structures. These small movements are apparently required for optimal interactions with the adenine moiety of the ligand. Tyr32 is involved in a stacking interaction with the adenine base and the side chain of Arg14 moves inwards into the acyl binding groove and a weak hydrogen bond is formed with the adenine ring of the ligand. Also small adjustments are seen near the N-terminus of helix A3. In the apo structure solvent water molecules are bound in the acyl-CoA binding pocket.

The apo ACBP structure includes one Pb^{2+} ion and one Zn^{2+} ion. The Pb^{2+} ion is bound at a crystal contact and it is complexed to Glu69 and Glu61 of a neighboring molecule, respectively. These side chains are not near the acyl-CoA binding pocket. However, in the hACBP-myristoyl-CoA complex form, Glu61 of molecule A is at the interface of the dimer of the asymmetric unit, where it is hydrogen bonded to Tyr32 of molecule B, which is a key residue in defining the adenine binding pocket. The Zn^{2+} ion of the apo ACBP structure is also bound at a crystal contact, complexed to the side chains of Glu11/His15 and Glu11/His15 of a neighboring molecule, respectively.

The Hexameric Myristoyl-CoA-Human L-ACBP Complex is Stabilized by a Zn^{2+} Cluster

The crystals of the complexed hL-ACBP were obtained by cocrystallization with $ZnCl_2$ and myristoyl-CoA at pH 6.5, resulting in two molecules per asymmetric unit. These two molecules (molecules A and B) are related by translational symmetry, not by a local twofold axis. Both molecules are liganded. The folds of the two molecules are very similar as shown in Figure 3(C). Molecule A is near a crystallographic three-fold symmetry axis, which generates a trimer of three A molecules, and together with the three B molecules, a hexameric assembly is formed (Figs. 4 and 5). The three A molecules at the centre of this hexamer interact with each other directly but additional stabilizing interactions occur indirectly via a cluster of seven Zn^{2+} ions.

The Zn^{2+} cluster resides on a threefold symmetry axis and consists of three crystallographically unique Zn^{2+} ions. This Zn^{2+} cluster is stabilized by a sulfate ion in the centre and nine surrounding phosphate groups of the six interacting 3′-phosphate-AMP moieties (molecules D1 and P1 and their three crystallographically related copies) (Fig. 5). Each of the Zn^{2+} ions is tetrahedrally coordinated by oxygen atoms, as seen in other Zn^{2+} complexes, and the Zn-O distances agree with published data.[29] The Zn^{2+} ions are not coordinated to water. Some disorder is observed in the cluster; for example, some Zn^{2+} ions do not have full occupancy and also the sulfate in its centre is disordered, as it is not precisely positioned on the threefold axis.

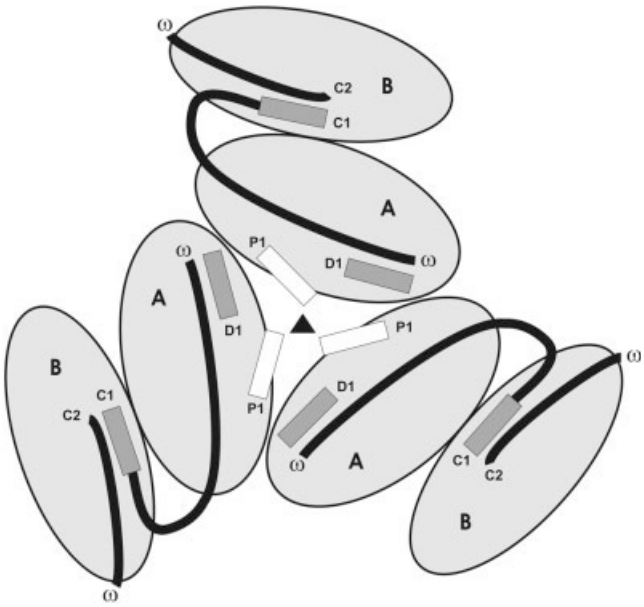

Fig. 4. Schematic representation of the hexameric assembly around the Zn^{2+} cluster. Protein chains A and B are labeled together with the ligand molecules. The ω-ends of the fatty acyl moieties of the ligands are indicated. The 3′-phosphate-AMP molecules in their classical binding pockets are shown as grey rectangles and the additional 3′-phosphate-AMP fragment (P1 having only weak interactions with the protein) as white rectangles. The central triangle represents the Zn^{2+} cluster assembled at the threefold symmetry axis.

One of the two unique 3′-phosphate-AMP moieties (D1) of the Zn^{2+} cluster binds to the A molecule in the classical mode (Fig. 2), whereas the second unique 3′-phosphate-AMP moiety (P1) binds in a nonconventional mode (Fig. 5). This unique Zn^{2+}/3′-phosphate-AMP complex stabilizes the trimeric assembly of the three A molecules; as each A molecule is additionally interacting with a B molecule, a hexameric arrangement of six ACBP molecules is generated (Figs. 4 and 5).

In this hexameric complex, altogether four myristoyl-CoA molecules (or at least their 3′-phosphate-AMP or acyl moieties) are bound per dimer of the asymmetric unit. Only one complete myristoyl-CoA molecule is seen (C1), which is bound between molecules A and B. This completely ordered molecule is bound with its 3′-phosphate-AMP moiety to molecule B and with its acyl part to molecule A. To molecule B is also bound an acyl-CoA fragment, being the β-mercaptoethylamine part plus the acyl tail, referred to as molecule C2, whereas to molecule A two 3′-phosphate-AMP moieties are bound: molecule D1 (bound in the classical way) and molecule P1. The latter 3′-phosphate-AMP moiety is only loosely interacting with the protein part of molecule A, as it is mainly stacked on the fatty acid tail of the C1 myristoyl-CoA molecule (Fig. 5). There is no electron density for the acyl-phosphopantetheine parts of molecules D1 and P1, suggesting that these fragments are disordered. Alternatively, the 3′-phosphate-

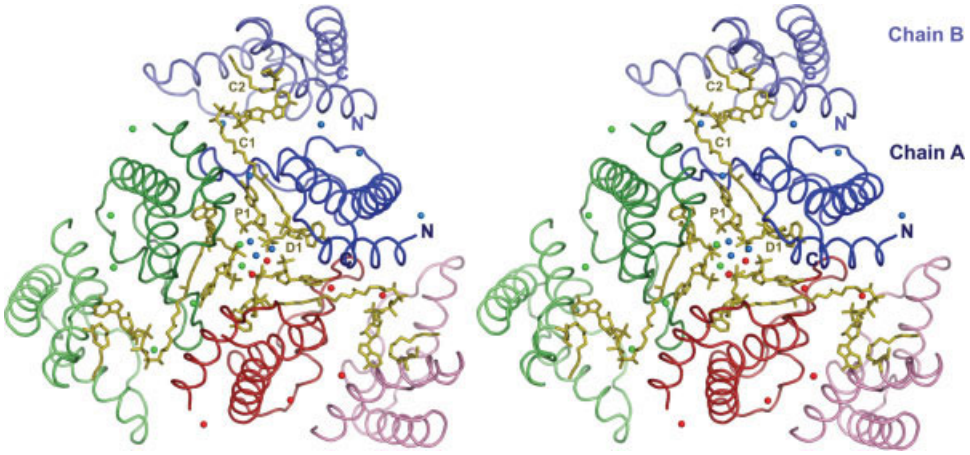

Fig. 5. The hL-ACBP-myristoyl-CoA hexamer. The organization of the three myristoyl-CoA-linked protein dimers around the Zn^{2+} cluster is shown. The three A chains (nearest to the Zn^{2+} cluster) are shown as dark red, dark green, and dark blue C^{α}-traces whereas the corresponding B chains of the dimers are colored light red, light green, and light blue. The Zn^{2+} ions of each asymmetric unit are colored as red, green, and blue spheres, respectively. The ligand molecules C1, C2, D1, and P1 are shown as yellow sticks. For clarity, the sulfate ion in the centre of the Zn^{2+} cluster is not shown.

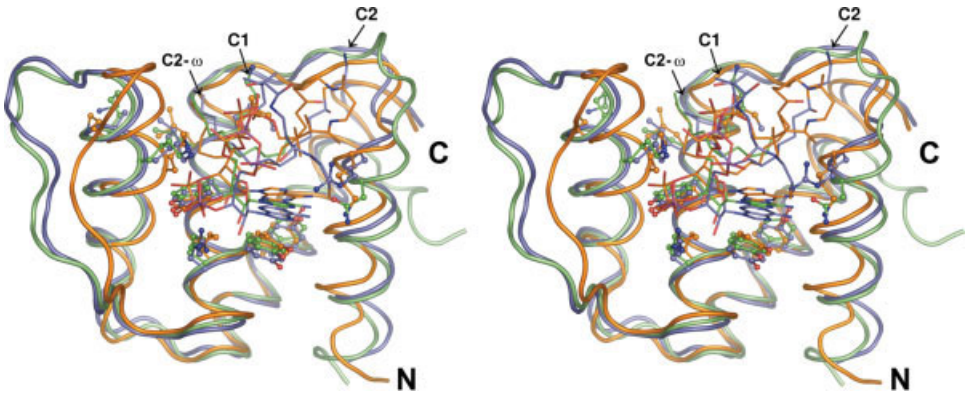

Fig. 6. Superimposition of the liganded human (chain B, blue), bovine (orange), and *P. falciparum* (green) ACBP structures. The ligand molecules and their contacting residues (Fig. 1) are shown as a stick model and are colored according to the corresponding backbone color. The ligands of the hL-ACBP are labeled. The acyl chain terminus of the ligand C1 is omitted for clarity.

AMP fragments present in the crystallization solution, as shown by the mass spectroscopy, have been incorporated in the crystallized complex.

The hexameric arrangement is not only stabilized by the Zn^{2+} ions of the Zn^{2+} cluster but also by two other Zn^{2+}-ligand interactions (with molecule P1 and molecule C1, respectively), as well as by two different Zn^{2+}-mediated interactions between molecule A and molecule B (Fig. 5). The eighth unique Zn^{2+} ion is bound at a crystal contact, stabilizing the interactions between two hexamers. The latter Zn^{2+} ion is complexed to Glu69, like the Pb^{2+} ion in the apo structure, although the crystal contacts are different, as the Zn^{2+} ion is bridged to Glu68 (of molecule A of a crystallographically related complex), whereas in the apo structure the Pb^{2+} ion is complexed to another glutamate (Glu61) of a neighboring molecule. The two Zn^{2+} ions bridging between molecule A and molecule B of the dimer of the complex (Zn1 and Zn5) are well defined in the map. Zn1 bridges from His31 (molecule A) to Glu7 (molecule B) and Zn5 bridges from Glu23 (molecule A) to Glu11/His15 (molecule B). Zn5 is at the same site as the Zn^{2+} ion seen in the apo structure; however, the latter Zn^{2+} ion is bridged to another side chain stabilizing, therefore, a different crystal contact as compared with the complexed crystal form. The Zn1 and Zn5 ions stabilize the dimer of the asymmetric unit of the complexed crystal form.

Comparison of the hL-ACBP, bL-ACBP, and Pf-ACBP Complexes

The 3′-phosphate-AMP moiety binds to molecule B essentially as in the classical mode as described for bL-ACBP and Pf-ACBP (Fig. 6). In bL-ACBP and Pf-ACBP, only one molecule of acyl-CoA is bound per ACBP molecule in the characteristically spiral conformation, whereas in hL-ACBP the ligands bound to an individual ACBP molecule originate from two different ligand molecules. It can be seen that the 3′-phosphate-AMP moiety in all three

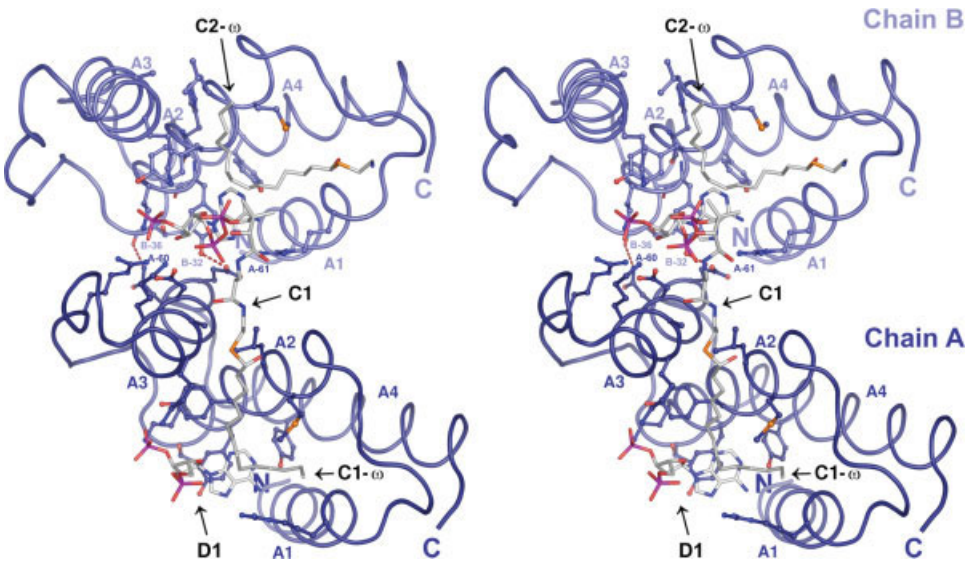

Fig. 7. The dimeric binding mode of the hL-ACBP-myristoyl-CoA complex. Chain A is shown in dark blue and chain B in light blue with helices labeled as in Figures 1 and 2. The 3′-phosphate-ribose moiety of the ligand molecule C1 is also hydrogen bonded to the side chains of chain A: to Arg44 and Lys53 (3′-phosphate moiety) and to Asp57 (ribose moiety). The two hydrogen bonding interactions between chain A and chain B are highlighted by dotted lines (between Asn60 (A) and Thr36 (B), and between Glu61 (A) and Tyr32 (B)). Also shown are the side chains of the residues contacting the ligand (also highlighted in Fig. 1).

structures is bound in the same way and the important side chain interactions are conserved (Fig. 6). In all three structures the ω-end of the acyl chain is near the N-termini of helices A2 (near residues 25 and 26) and A3 (near residues 54 and 55), but in the hL-ACBP molecule B this fatty acyl moiety belongs to a second myristoyl-CoA molecule. It has been noted[12] that in bL-ACBP a possible binding tunnel is present between the N-termini of helices A2 and A3, whereas in PfACBP this tunnel is absent. In hL-ACBP, the binding tunnel is also present, and in the A molecule it is actually used for binding the β-mercaptoethylamine part of the full length C1 myristoyl-CoA molecule (Figs. 3 and 7), as is discussed in the next section.

Concerning differences in the protein structure, it can be noted that in bL-ACBP, the N-terminus of helix A3 moves toward the binding pocket, as compared with hL-ACBP and Pf-ACBP, making the bL-ACBP structure more compact. Other structural differences are seen near the C-terminus of helix A1. This region forms the binding groove for the acyl chain (as well as for the β-mercaptoethanol part of the pantetheine moiety). Pf-ACBP has a unique two-residue insertion in this loop (Figs. 1 and 6) and the structural differences of this loop region, as well as sequence variations near the adjacent tunnel between the N-termini of helices A2 and A3, correlate with differences in acyl length specificity between bL-ACBP, hL-ACBP, and Pf-ACBP.[12]

Myristoyl-CoA Binding Between the Two Molecules A and B

In the myristoyl-CoA-hL-ACBP complex, only one complete myristoyl-CoA molecule is seen (C1), which is bound between molecules A and B (Fig. 7). This completely ordered molecule is bound with its CoA end to molecule B and with its acyl part to molecule A. The 3′-phosphate moiety of C1 hydrogen bonds to the conserved Tyr29, Lys33, and Lys55 residues of molecule B. Lys55 is additionally salt bridged to the pyrophosphate moiety. In addition to these interactions present in the other known structures of ACBP complexes, there are additional hydrogen bonds from monomer A to molecule C1: from Arg44 and Lys53 to the 3′-phosphate, and from Asp57 to the ribose hydroxyl group. There exist also two strong direct hydrogen bonds between the protein molecules A and B: between Asn60 (side chain, molecule A) and Thr36 (main chain, molecule B); and between Glu61 (side chain, molecule A) and Tyr32 (side chain, molecule B), as depicted in Fig. 7. The pantothenic acid moiety of the C1 myristoyl-CoA does not have direct contacts with side chains of either molecule A or B, whereas the β-mercaptoethylamine part is bound in the tunnel between the N-termini of helices A2 and A3 (molecule B) and the ω-end of C1 is bound in the classical fatty acid moiety binding groove (molecule A) as observed in bL-ACBP and Pf-ACBP (Figs. 2 and 6). Interestingly, the ω-end of the acyl chain binds in this groove in a reversed orientation, as compared with classical monomeric binding (Fig. 2), and as is also seen in the complex of molecule B and ligand C2 (Fig. 3).

Correlated with this reverse mode of binding are structural differences between molecules A and B in the loop region between helices A1 and A2 (Fig. 3). In particular, this concerns side chains Arg14, Lys19, and Met25. These structural differences make the binding groove somewhat narrower in the presence of the ω-end of the acyl chain (reversed mode; C1 bound to monomer A), while in the classical mode (C2 bound to monomer B) the groove is

wider, as is also clearly visible in Figure 3(A). As is also shown in Figure 3, in the classical mode of binding the conformation of this loop is identical with the one seen in the apo hL-ACBP structure. It is of interest to point out that a reversed mode of binding of the lipid molecule has also been seen in at least one other lipid–protein complex, being a lipid-SCP2 complex. In this case it was also found that the hydrophobic moieties of two different lipids are bound at opposite ends of the same binding groove.[30]

DISCUSSION

How is the dimeric complex as seen in this structure of the myristoyl-CoA-hL-ACBP complex formed? It is possible to propose at least one mechanism. First, myristoyl-CoA binds with its adenine part as seen in molecule B. If the fatty acyl chain binds in the binding groove of the same polypeptide, the classical monomeric complex is formed. Alternatively, the fatty acyl part is pointing into solution and subsequently binds in the fatty acyl binding groove of the second molecule (represented by molecule A in this structure). This dimeric mode of binding is facilitated by the interaction of the ribose-3′-phosphate part with the extra binding surface of molecule A (formed by residues Arg44, Lys53, and Asp57) (Fig. 7). Subsequently, the remaining empty regions of the binding pockets are filled up by other myristoyl-CoA molecules (or their fragments) and after that the hexamer, as seen in the crystallized form, is stabilized by the Zn^{2+} cluster. In particular, ligand molecule P1 of the Zn^{2+} cluster interacts with the extended fatty acid tail of C1 and stabilizes its dimeric binding mode (Fig. 5). The two alternative modes of binding of the acyl moiety suggest high mobility for the pantetheine moiety. This correlates well with the structure of liganded Pf-ACBP in which the pantetheine moiety is invisible in the electron density map because of disorder.

Arg44, Lys53, and Asp57 of the extra binding surface on molecule A are fully conserved in L-ACBP (there is only one exception of Lys53 changed into an arginine).[4] These residues are surface residues and consequently their full conservation cannot be understood from the classical mode of ligand binding. This suggests that the alternative, dimeric mode of binding of the fatty acyl-CoA molecule, as seen in the myristoyl-CoA-hL-ACBP complex, might be functionally relevant. Also important for this dimeric mode of binding is the tunnel between the N-termini of helices A2 and A3, which is present in the structures of both bovine[12] and human ACBP.

The dimeric mode of binding of the myristoyl-CoA on the ACBP has not been seen before. However, ACBP is known to be able to transfer its acyl-CoA directly to enzymes catalyzing acyl-CoA modifications.[31,32] The acyl-CoA ACBP complex is the substrate of these enzymes and after formation of the ACBP-enzyme complex, the acyl-CoA molecule is transferred via an unknown mechanism from the ACBP molecule to the enzyme.

This dimeric mode of binding is also an interesting model for the exchange of membrane-bound acyl-CoA and ACBP. Studies of the interaction of ACBP with membranes showed that ACBP can bind to membranes and desorb membrane-bound acyl-CoA.[33] In the proposed mechanism, acyl-CoA has its fatty acyl chain buried in the outer membrane leaf and the CoA end is exposed to the solvent phase. Desorption from the membrane is initiated by binding of the CoA end to ACBP leaving the acyl chain binding groove initially empty. The binding interactions between ACBP and 3′-phosphate group are apparently strong enough to keep ACBP associated on the membrane by being anchored to CoA. Alternatively, the binding is stabilized by an acyl chain flipped out from the membrane and binding in the hydrophobic groove in a similar way as ligand C2 stabilizes the binding of the CoA head group of C1 in molecule B (Fig. 7).

CONCLUSIONS

This structural analysis of unliganded and liganded human ACBP shows that human ACBP has the same binding pocket as previously characterized for bovine ACBP and *P. falciparum* ACBP. The liganded form of human ACBP has been crystallized in the presence of 20 m*M* Zn^{2+} and 1.8 m*M* myristoyl-CoA. The asymmetric unit of these liganded crystals contains two molecules of ACBP. The binding pocket of each of these two ACBP molecules has a bound 3′-phosphate-AMP moiety and a bound fatty acyl-CoA moiety, originating from two different myristoyl-CoA molecules. It is also shown that one myristoyl-CoA molecule (molecule C1) can bind such that it is shared between two ACBP molecules; its 3′-phosphate-AMP head group binds to ACBP molecule B, and its fatty acid moiety binds in the acyl binding groove of an adjacent molecule A. In this dimeric mode of binding, the acyl moiety is bound in the opposite direction when compared with the classical, monomeric mode of binding, whereas its 3′-phosphate-AMP moiety is bound in the classical way. This dimeric mode of binding is stabilized by the Zn^{2+} cluster and the P1 3′-phosphate AMP fragment. Further solution studies are required to verify if this dimeric mode of binding is physiologically relevant. ACBP binds acyl-CoA with very high affinity (K_D = 1–5 n*M*), which suggests that a ligand transfer mechanism from ACBP to acyl-CoA consuming enzymes must exist. The observed dimeric mode of binding might help to understand the mechanism by which long chain fatty acyl-CoAs are exchanged between fatty acyl-CoA ACBP complexes and target molecules like acyl-CoA processing enzymes or membranes. Electrospray mass spectroscopy has shown that the acyl chain of palmitoyl-CoA bound to ACBP flips out upon removal of water in the spray process.[34] A similar event could occur by creation of hydrophobic environment at the contact site between the acyl-CoA ACBP complex and the acyl-CoA consuming enzyme. The interaction of ACBP with membranes and the removal of acyl-CoA from the membrane by ACBP[33] could be facilitated by formation of an ACBP-membrane complex with an acyl chain flipped out of the membrane, similarly as the binding of the fatty acid tail moiety of ligand C2 stabilizes the binding of the 3′-phosphate AMP moiety of the myristoyl-CoA molecule C1. In summary, the

crystal structure of this hL-ACBP myristoyl-CoA complex suggests that the acyl-CoA molecule can be bound with its 3′-phosphate-AMP part to ACBP whereas the fatty acid moiety is available for interactions with binding pockets present in other proteins.

ACKNOWLEDGMENTS

The skillful support by the staff at the beam lines X11 (EMBL-Hamburg) of DESY and ID14-4 (ESRF) is gratefully acknowledged. The authors thank Dr. U. Bergmann (Department of Biochemistry, University of Oulu) for carefully carrying out the mass spectroscopy experiments. The coordinates of the unliganded and liganded hL-ACBP structures have been deposited in the RCSB-PDB with entry codes 2FJ9 and 2CB8, respectively.

REFERENCES

1. Faergeman NJ, Knudsen J. Role of long-chain fatty acyl-CoA esters in the regulation of metabolism and in cell signalling. Biochem J 1997;323:1–12.
2. Knudsen J, Burton M, Faergeman NJ. Long chain acyl-CoA esters and acyl-CoA binding protein (ACBP) in cell function. In: Bittar EE, editor. Advances in molecular and cell biology. Oxford: Elsevier; 2004. pp 123–153.
3. Owens GP, Sinha AK, Sikela JM, Hahn WE. Sequence and expression of the murine diazepam binding inhibitor. Brain Res Mol Brain Res 1989;6:101–108.
4. Burton M, Rose TM, Faergeman NJ, Knudsen J. Evolution of the acyl-CoA binding protein (ACBP). Biochem J 2005;392:299–307.
5. Chye ML, Huang BQ, Zee SY. Isolation of a gene encoding Arabidopsis membrane-associated acyl-CoA binding protein and immunolocalization of its gene product. Plant J 1999;18:205–214.
6. Geisbrecht BV, Zhang D, Schulz H, Gould SJ. Characterization of PECI, a novel monofunctional Delta(3), Delta(2)-enoyl-CoA isomerase of mammalian peroxisomes. J Biol Chem 1999;274: 21797–21803.
7. Chye ML, Li HY, Yung MH. Single amino acid substitutions at the acyl-CoA binding domain interrupt ^{14}C-palmitoyl-CoA binding of ACBP2, an Arabidopsis acyl-CoA binding protein with ankyrin repeats. Plant Mol Biol 2000;44:711–721.
8. Pearson MA, Reczek D, Bretscher A, Karplus PA. Structure of the ERM protein moesin reveals the FERM domain fold masked by an extended actin binding tail domain. Cell 2000;101:259–270.
9. Mogensen IB, Schulenberg H, Hansen HO, Spener F, Knudsen J. A novel acyl-CoA binding protein from bovine liver: effect on fatty acid synthesis. Biochem J 1987;241:189–192.
10. Andersen KV, Ludvigsen S, Mandrup S, Knudsen J, Poulsen FM. The secondary structure in solution of acyl-coenzyme A binding protein from bovine liver using 1H nuclear magnetic resonance spectroscopy. Biochemistry 1991;30:10654–10663.
11. Kragelund BB, Andersen KV, Madsen JC, Knudsen J, Poulsen FM. Three-dimensional structure of the complex between acyl-coenzyme A binding protein and palmitoyl-coenzyme A. J Mol Biol 1993;230:1260–1277.
12. van Aalten DM, Milne KG, Zou JY, Kleywegt GJ, Bergfors T, Ferguson MA, Knudsen J, TA Jones. Binding site differences revealed by crystal structures of *Plasmodium falciparum* and bovine acyl-CoA binding protein. J Mol Biol 2001;309:181–192.
13. Fieber W, Kragelund BB, Meldal M, Poulsen FM. Reversible dimerization of acid-denatured ACBP controlled by helix A4. Biochemistry 2005;44:1375–1384.
14. Faergeman NJ, Sigurskjold BW, Kragelund BB, Andersen KV, Knudsen J. Thermodynamics of ligand binding to acyl-coenzyme A binding protein studied by titration calorimetry. Biochemistry 1996;35:14118–14126.
15. Kragelund BB, Poulsen K, Andersen KV, Baldursson T, Kroll JB, Neergard TB, Jepsen J, Roepstorff P, Kristiansen K, Poulsen FM, Knudsen J. Conserved residues and their role in the structure, function, and stability of acyl-coenzyme A binding protein. Biochemistry 1999;38:2386–2394.
16. Mandrup S, Hojrup P, Kristiansen K, Knudsen J. Gene synthesis, expression in *Escherichia coli,* purification and characterization of the recombinant bovine acyl-CoA-binding protein. Biochem J 1991; 276:817–823.
17. Smith DR, Kahng MW, Quintanilla-Vega B, Fowler BA. High-affinity renal lead-binding proteins in environmentally-exposed humans. Chem Biol Interact 1998;14:39–52.
18. Jancarik K, Kim SH. Sparse matrix sampling: a screening method for crystallization of proteins. J Appl Crystallogr 1991;24:409–411.
19. Otwinowski Z, Minor W. Processing of X-ray diffraction data collected in oscillation mode. In: Carter CW, Sweet RM, editors. Methods in enzymology. San Diego: Academic Press; 1997. pp 307–326.
20. Brunger AT. Assessment of phase accuracy by cross validation: the free R value. Methods and applications. Acta Crystallogr D Biol Crystallogr 1993;49:24–36.
21. Kabsch W. Automatic processing of rotation diffraction data from crystals of initially unknown symmetry and cell constants. J Appl Crystallogr 1993;26:795–800.
22. Brunger AT, Adams PD, Clore GM, DeLano WL, Gros P, Grosse-Kunstleve RW, Jiang JS, Kuszewski J, Nilges M, Pannu NS, Read RJ, Rice LM, Simonson T, Warren GL. Crystallography and NMR system: a new software suite for macromolecular structure determination. Acta Crystallogr D Biol Crystallogr 1998;54:905–921.
23. Perrakis A, Morris R, Lamzin VS. Automated protein model building combined with iterative structure refinement. Nat Struct Biol 1999;6:458–463.
24. Jones TA, Zou JY, Cowan SW, Kjeldgaard. Improved methods for building protein models in electron density maps and the location of errors in these models. Acta Crystallogr A 1991;47:110–119.
25. Laskowski RA, MacArthur MW, Moss DS, Thornton JM. PROCHECK: a program to check the stereochemical quality of protein structures. J Appl Cryst 1993;26:283–291.
26. Vriend G. WHAT IF: a molecular modeling and drug design program. J Mol Graph 1990;8:52–56.
27. Murshudov GN, Vagin AA, Dodson EJ. Refinement of macromolecular structures by the maximum-likelihood method. Acta Crystallogr D Biol Crystallogr 1997;53:240–255.
28. Winn MD, Isupov MN, Murshudov GN. Use of TLS parameters to model anisotropic displacements in macromolecular refinement. Acta Crystallogr D Biol Crystallogr 2001;57:122–133.
29. Harding MM. Geometry of metal-ligand interactions in proteins. J Am Chem Soc 2001;57:401–411.
30. Dyer DH, Lovell S, Thoden JB, Holden HM, Rayment I, Lan Q. The structural determination of an insect sterol carrier protein-2 with a ligand-bound C16 fatty acid at 1.35-A resolution. J Biol Chem 2003;278:39085–39091.
31. Abo-Hashema KA, Cake MH, Lukas MA, Knudsen J. The interaction of acyl-CoA with acyl-CoA binding protein and carnitine palmitoyltransferase I. Int J Biochem Cell Biol 2001;33:807–815.
32. Chao H, Zhou M, McIntosh A, Schroeder F, Kier AB. ACBP and cholesterol differentially alter fatty acyl CoA utilization by microsomal ACAT. J Lipid Res 2003;44:72–83.
33. Simonsen AC, Jensen UB, Faergeman NJ, Knudsen J, Mouritsen OG. Acyl-coenzyme A organizes laterally in membranes and is recognized specifically by acyl-coenzyme A binding protein. FEBS Lett 2003;552:253–258.
34. Robinson CV, Chung EW, Aplin RT, Dobson CM, Kragelund BB, Poulsen FM, Knudsen J. Probing the nature of noncovalent interactions by mass spectrometry. A study of protein-CoA ligand binding and assembly. J Am Chem Soc 1996;118:8646–8653.